

Dark matter vs. astrophysics in the interpretation of AMS-02 electron and positron data

Mattia Di Mauro^{a,b} Fiorenza Donato^{a,b} Nicolao Fornengo^{a,b} Andrea Vittino^{a,b}

^aDepartment of Physics, University of Torino, via P. Giuria 1, 10125 Torino, Italy

^bIstituto Nazionale di Fisica Nucleare, via P. Giuria 1, 10125 Torino, Italy

E-mail: mattia.dimauro@to.infn.it, donato@to.infn.it, fornengo@to.infn.it,
vittino@to.infn.it

Abstract. We perform a detailed quantitative analysis of the recent AMS-02 electron and positron data. We investigate the interplay between the emission from primary astrophysical sources, namely Supernova Remnants and Pulsar Wind Nebulae, and the contribution from a dark matter annihilation or decay signal. Our aim is to assess the information that can be derived on dark matter properties when both dark matter and primary astrophysical sources are assumed to jointly contribute to the leptonic observables measured by the AMS-02 experiment. We investigate both the possibility to set robust constraints on the dark matter annihilation/decay rate and the possibility to look for dark matter signals within realistic models that take into account the full complexity of the astrophysical background. Our results show that AMS-02 data enable to probe efficiently vast regions of the dark matter parameter space and, in some cases, to set constraints on the dark matter annihilation/decay rate that are comparable or even stronger with respect to the ones that can be derived from other indirect detection channels. For DM annihilation into muons, the bounds leave room for a possible joint DM+astro interpretation of the data, with a DM mass in the 50–80 GeV range (depending on the pulsars modeling) and an annihilation cross section in the range $(0.7 \div 3)$ times the thermal cross section.

Contents

1	Introduction	1
2	Contributions to the e^+e^- flux	2
2.1	Secondaries	2
2.2	Supernova Remnants	3
2.3	Pulsar Wind Nebulae	3
2.4	Dark Matter	4
3	Transport in the galaxy and in the Heliosphere	4
4	Analysis and results	5
4.1	The purely astrophysical interpretation	6
4.2	Adding dark matter to the picture	9
4.2.1	Constraints on dark matter annihilation/decay	10
4.2.2	Allowed regions in the DM parameters space	10
4.2.3	Varying the astrophysical modeling	13
5	Conclusions	18

1 Introduction

Dark matter (DM) stands out as one of the most intriguing challenges in physics. While gravitational effects of this elusive substance are manifest in a variety of observables, ranging from the astrophysical to the cosmological scale, an indisputable non-gravitational evidence of its existence has yet to be unveiled. Among the techniques developed to pursue the search of DM non-gravitational imprints, there is the so-called indirect detection, which consists in the attempt to reveal a signal that can be the outcome of a DM pair annihilation or decay event and that can possibly manifest its presence as an exotic component in cosmic rays (CRs).

In the framework of this searching strategy, a preeminent role is played by the analysis of the fraction of antimatter in the flux of charged CRs. In particular, in recent years, the observations performed by the PAMELA satellite of a steep rise in the energy spectrum of the positron fraction [1] has been interpreted by many authors as a possible evidence for the existence of a leptophilic TeV-scale WIMP (see, for example, Refs. [2–8]). However, as stressed in several works, plausible astrophysical mechanisms able to generate such a rise in the positron fraction can be conceived: while the most widely known example invokes Pulsar Wind Nebulae (PWNe) or Supernova Remnants (SNRs) or a combination of both as sources of primary e^\pm [9–12], it has also been shown that the secondary production of e^\pm *within* the shock region of SNRs provides a perfectly viable mechanism to explain observations [13, 14]. Several features that characterize these interpretations of the PAMELA excess have been investigated in a series of recent works (see, for example, Refs. [15–23]) in connection to the data delivered by the AMS-02 experiment.

In a previous work [24] we have carried out a detailed and quantitative analysis of the four observables measured by the AMS-02 experiment (electron flux, positron flux, total leptonic flux and positron fraction) within a purely astrophysical model for e^\pm generation. In

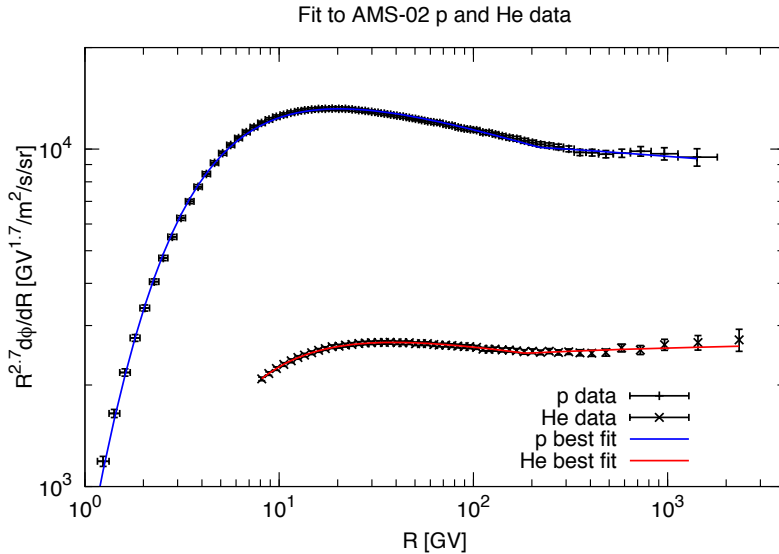


Figure 1. Fit to the proton and helium fluxes measured by AMS-02: the black points denote experimental data, while the blue and red solid lines represent our best fits.

this paper our purpose is to extend this quantitative study to include also a DM contribution: the aim is to assess the constraints on DM obtainable within a model in which the astrophysical background is included and modeled in a realistic way. In particular, we stress that, differently from Ref. [24] where we used an 8% error on the AMS-02 measured fluxes, we are now making full profit of the recently published AMS-02 Collaboration data, which report smaller uncertainties on their whole set of observables.

The paper is organised as follows: in Section 2 we briefly illustrate the various contributions to the electron and positron fluxes, while in Section 3 we describe the framework that we use to model the transport of positrons and electrons across the Galaxy and the heliosphere. In Section 4, we present the methods that we use for the different parts of our analysis and the results that we obtain. Finally, in Section 5 we derive our conclusions.

2 Contributions to the e^+e^- flux

In this Section, we briefly review the role of the main sources that contribute to the four observables measured by the AMS-02 experiment. For a more detailed description of all the astrophysical contributions (primary and secondary) we address the reader to Ref. [24].

2.1 Secondaries

Electrons and positrons can be generated in spallation reactions that involve primary CRs, in particular proton and Helium nuclei, impinging on the nuclei that populate the interstellar medium (ISM), the dominant component of which being represented by Hydrogen. The source term related to this contribution is:

$$q_{e^\pm}(\vec{x}, E_e) = 4\pi n_{\text{ISM}}(\vec{x}) \int dE_{\text{CR}} \Phi_{\text{CR}}(\vec{x}, E_{\text{CR}}) \frac{d\sigma}{dE_e}(E_{\text{CR}}, E_e), \quad (2.1)$$

where the quantity n_{ISM} represents the density of target nuclei in the ISM, Φ_{CR} is the flux of the primary CR species and the term $d\sigma/dE_e$ stands for the differential inclusive cross section for the electron/positron production in the spallation reaction under study.

By following the same approach outlined in Ref. [24], we set the primary CR fluxes by fitting the recent AMS-02 measurements of the proton [25] and Helium [26] fluxes with the following interstellar spectra:

$$\Phi_{\text{CR}}(R) = \begin{cases} A\beta^P R^{-P_1} & \text{for } R \leq R_{\text{break}}, \\ A\beta^P R_{\text{break}}^{-P_1+P_2} R^{-P_2} & \text{for } R > R_{\text{break}}, \end{cases} \quad (2.2)$$

where $R = pc/eZ$ and β denote, respectively, the rigidity and the velocity of the particle under consideration. We allow for the presence of a spectral break at a rigidity R_{break} to be determined through the fitting procedure. For the best-fit configuration the values of the parameters are: $A = 26700 \pm 500 \text{ m}^{-2}\text{s}^{-1}\text{sr}^{-1}(\text{GeV}/n)^{-1}$, $P = 7.2 \pm 0.4$, $P_1 = 2.877 \pm 0.004$, $P_2 = 2.748 \pm 0.013$ and $R_{\text{break}} = 220 \pm 22 \text{ GV}$ for the proton and $A = 4110 \pm 80 \text{ m}^{-2}\text{s}^{-1}\text{sr}^{-1}(\text{GeV}/n)^{-1}$, $P = 3.5 \pm 0.7$, $P_1 = 2.793 \pm 0.004$, $P_2 = 2.689 \pm 0.013$ and $R_{\text{break}} = 187 \pm 18 \text{ GV}$ for the Helium, the Fisk solar modulation potential being set to 700 MV. The best fit to the combined proton and Helium data has a reduced chi-square ($\chi^2/\text{d.o.f.}$) equal to 0.43, which corresponds to a p -value and significance of 3.1×10^{-9} and 5.9σ , respectively. The proton and Helium fluxes for this best-fit configuration are shown, together with the AMS-02 measurements in Fig. 1.

Concerning the inclusive production cross sections $d\sigma/dE_e$, for the case of p-p collisions we use the parameterization described in Ref. [27], while to model processes involving Helium nuclei, either as the incoming particle or the target, we resort to the empirical prescriptions illustrated in Ref. [28].

2.2 Supernova Remnants

SNRs are usually thought to play the dominant role in accelerating charged cosmic rays within the Galaxy. This acceleration is realised through the propagation of non-relativistic shock waves that are produced by the star explosion. The typical SNR injected spectra have the shape of a power-law with a cut-off at large energies:

$$Q(E) = Q_{0,\text{SNRs}} \left(\frac{E}{E_0} \right)^{-\gamma_{\text{SNRs}}} \exp\left(-\frac{E}{E_c}\right), \quad (2.3)$$

being $Q_{0,\text{SNRs}}$ the normalization of the spectrum, γ_{SNRs} the spectral index and E_c the cut-off energy. As it has been extensively discussed in [24], the parameters $Q_{0,\text{SNRs}}$ and γ_{SNRs} can be inferred from the study of the radio emission measured in the region of the sky that hosts the SNR, while E_c is expected to lie at the TeV range [29–33]. In the analysis that will be described in the following Sections of the paper, we assume $E_c = 2 \text{ TeV}$. Let us remark that, however, as far as E_c is beyond the maximal energy that is measured by AMS-02, the exact value of this parameter does not affect our results. Finally, every time that, in our investigations, we will need to use SNRs parameters we will resort to the Green catalogue [34], which is the most complete catalogue of Galactic SNRs.

2.3 Pulsar Wind Nebulae

Also pulsars are expected to generate a flux of electrons and positrons through a mechanism known as spin-down emission (for a description of which we address the reader to Refs. [35–43]). In a few simple words, this mechanism is a consequence of electrons and positrons being

torn away from the surface of the neutron star by the strong electric field generated by the pulsar spinning. These charged particles gather in a sort of wind that surrounds the pulsar and then are released in the ISM at the disruption of this nebula. Because of this injection mechanism, which is fast and followed by a weak residual energy emission, PWNe can be considered as burst-like sources of e^\pm .

The spectrum of the e^\pm injected by a PWN in the ISM has the same expression as the one in Eq. 2.3 associated to SNRs. As outlined in [24], the normalization of this spectrum is related to the efficiency η_{PWNe} with which the PWN can convert its spin down energy into the production of e^\pm pairs:

$$\int_{E_{\min}}^{\infty} dE E Q(E) = \eta_{\text{PWNe}} W_0, \quad (2.4)$$

where the quantity W_0 represents the total spin-down energy which, in terms of the present age of the pulsar t_* and the typical pulsar decay time τ_0 can be expressed as:

$$W_0 \approx \tau_0 \dot{E} \left(1 + \frac{t_*}{\tau_0}\right)^2. \quad (2.5)$$

The most complete list of PWNe is represented by the ATNF catalogue [44]. As it will be widely discussed in the following, we will use it as a reference for all the PWN parameters.

2.4 Dark Matter

Positrons and electrons can also be the result of the pair annihilation or decay of DM particles. The source terms associated to these contributions are:

$$\begin{aligned} \mathcal{Q}_{\text{ann}}(\vec{x}, E) &= \epsilon \left(\frac{\rho(\vec{x})}{m_{DM}}\right)^2 \sum_f \langle \sigma v \rangle_f \frac{dN_{e^\pm}^f}{dE}, \\ \mathcal{Q}_{\text{dec}}(\vec{x}, E) &= \left(\frac{\rho(\vec{x})}{m_{DM}}\right) \sum_f \Gamma_f \frac{dN_{e^\pm}^f}{dE}, \end{aligned} \quad (2.6)$$

where \vec{x} denotes Galactic position, ϵ being a factor that takes the value 1/2 or 1/4 for, respectively, a self-conjugate or non self-conjugate DM particle, while f denotes the Standard Model particles that can be produced in the annihilation or decay process and the functions $dN_{e^\pm}^f/dE$ represent the e^\pm energy spectrum generated in a single annihilation or decay process. The galactic DM halo, filled with particles with mass m_{DM} , follows a spatial density $\rho(\vec{x})$. We perform a model independent analysis which consists in assuming that the DM annihilation/decay occurs in a single channel. In particular, we will focus our attention on the five channels e^+e^- , $\mu^+\mu^-$, $\tau^+\tau^-$, $b\bar{b}$, W^+W^- . We model the energy spectra $dN_{e^\pm}^f/dE$ from Ref. [45]: we remind that these spectra have been computed by taking into account *electroweak correction* which, as stressed in [46] can play a non-negligible role in shaping the e^\pm emission when the DM mass is above the electroweak scale.

3 Transport in the galaxy and in the Heliosphere

After being injected by their source, electrons and positrons propagate across the ISM where spatial diffusion, convection, reacceleration and energy losses can shape their spectrum. To

model this transport and take into account these effects, we have to solve the transport equation:

$$\partial_t \mathcal{N} - \vec{\nabla} \cdot \left\{ K(E) \vec{\nabla} \mathcal{N} \right\} + \partial_E \left\{ \frac{dE}{dt} \mathcal{N} \right\} = \mathcal{Q}(E, \vec{x}, t), \quad (3.1)$$

where \mathcal{N} denotes the positron(electron) number density per unit energy while $\mathcal{Q}(E, \vec{x}, t)$ represents the source terms that were discussed in the previous Sections. The diffusion coefficient $K(E)$, which we assume to be space independent, is defined in the following way:

$$K(E) = \beta K_0 (R/1 \text{ GV})^\delta. \quad (3.2)$$

The term $\frac{dE}{dt}$ is given by the sum of the synchrotron energy loss term (which depends on the value of the Galactic magnetic field, for which, compatibly with Ref. [47], we have assumed an intensity of $2 \mu\text{G}$ ($3 \mu\text{G}$) for the regular (random) component) and the inverse Compton (IC) loss term (for which we have included a full relativistic treatment [48]). Additional energy loss processes, namely bremsstrahlung, ionization and Coulombian interactions on the ISM can be safely neglected.

In solving Eq. 3.1, we adopt the *two-zone diffusion model*, which has been extensively described in literature (see for example Ref [49]). In this paper we adopt the set of propagation parameters defined in the MED propagation model of Ref. [50]. For any further detail we address the reader to Ref. [48].

Lastly, for the solar modulation of the fluxes, we have used the usual force field approximation treated in Refs. [51, 52]. In this frameworks, the solar modulation depends on the value of the parameter ϕ , the so-called *Fisk potential*. As it will be discussed in the following, we will always determine ϕ directly from data.

4 Analysis and results

The AMS-02 Collaboration has recently published the results of their 30 months measurements of the full set of observables that are related to the physics of cosmic electrons and positrons, *i.e.*, the e^- and e^+ fluxes [53], the total $e^- + e^+$ flux [54] and the positron fraction $e^+/(e^- + e^+)$ [55]. Our main purpose in this Section is to test various possible interpretations of these experimental data.

The analyses are based on a global fit of the four aforementioned observables within several theoretical frameworks (described below), each one being characterized by a certain set of parameters $\{\theta_1, \dots, \theta_N\}$, whose total number N depend on the specific model under scrutiny. The N -dimensional parameters space of each model is sampled by means of a Markov Chain Monte Carlo (MCMC) scan performed with the COSMOMC package [56]. In order to determine the configuration of parameters providing the best agreement with AMS-02 measurements we assign to each N-tuple $\{\theta_1, \dots, \theta_N\}$ a chi-square estimator defined as:

$$\chi^2 = -\ln L = \sum_j \sum_i \frac{(f_i^j(\theta_1, \dots, \theta_N) - d_i^j)^2}{(\sigma_i^j)^2}, \quad (4.1)$$

where the indices j and i run over the four AMS-02 observables and the different energy bins, respectively. The quantities $f_i^j(\theta_1, \dots, \theta_N)$ represent the theoretical predictions while d_i^j stands for the observed experimental data values, which are affected by the experimental uncertainties σ_i^j .

η_{PWNe}	γ_{PWNe}	$Q_{0,\text{SNRs}}[10^{50} \text{ erg/s}]$	γ_{SNRs}	N_{Vela}
$0.0368^{+0.0011}_{-0.0014}$	$1.948^{+0.025}_{-0.022}$	$1.231^{+0.014}_{-0.028}$	$2.238^{+0.015}_{-0.013}$	$0.978^{+0.031}_{-0.130}$
$\chi^2/\text{d.o.f.} = 1.03$ and $p\text{-value} = 0.37$ (1.0σ)				

Table 1. Best-fit parameters for the *astro model*.

As already done in Ref. [24], we choose to test the different theoretical models by analyzing the entire set of observables measured by AMS-02: electron flux, positron flux, total $e^+ + e^-$ flux and positron fraction. In fact, even if, under a purely formal point of view, only two of them should be considered as truly independent, this is not the case in practice, since the four observables are the result of independent experimental analyses. Therefore, we believe that using the four datasets is a more robust way to check the consistency among the measurements and their agreement with the theoretical models that we consider.

Another point worth to be mentioned here is that in this analysis we choose to consider only data above 10 GeV. In fact, the sector relevant for the investigation of primary astrophysical e^\pm sources and of the corresponding DM contribution is the high energy part of the spectra. Considering that time-dependent solar modulation effects become increasingly important at lower energies, we decide to concentrate our analysis only on the high energy part, in order to avoid that the numerous AMS-02 energy bins at very low energy (which require detailed, although uncertain, solar modulation modeling) would drive the statistical significance of the fit to the part of the spectrum which is of least importance to the present analysis. Since the effect of transport in the heliosphere is still present up to few tens of GeV, we nevertheless consider solar modulation by applying the simple Fisk method (as discussed above): however, by concentrating on energies above 10 GeV we minimize the bias of the low-energy solar-modulation-dominated data bins. The choice of 10 GeV as the discriminating energy has been adopted as a trade off between the requirement of reducing the impact of solar modulation modeling and the interest to investigate the energy region where DM and primary sources start to emerge.

4.1 The purely astrophysical interpretation

In this paragraph, we follow the prescriptions presented in our previous work [24] and discuss our new analysis for a purely astrophysical interpretation of AMS-02 measurements. In brief, the model, which we label *astro model*, is composed by:

- **Secondary e^- and e^+ :** their flux is computed by using the source term introduced in Section 2.1. We recall that this component is fixed. In fact, its contribution depends on the primary CR fluxes and on the parameterization of the spallation cross sections, which we do not vary in our analysis. The secondary e^+ component is the dominant one at low energies, where it has been shown in Ref. [24] to perfectly reproduce the measured AMS-02 flux, within the chosen propagation model.
- **Primary e^- accelerated by SNRs:** for this contribution, which has been discussed in Section 2.2, we follow the approach outlined in Ref. [24], that consists in separating the total population of SNRs into two categories:
 - Far SNRs ($d > 3$ kpc): they are modeled as an average component with a spatial distribution taken from Ref. [64]. The sources that fall in this class share common

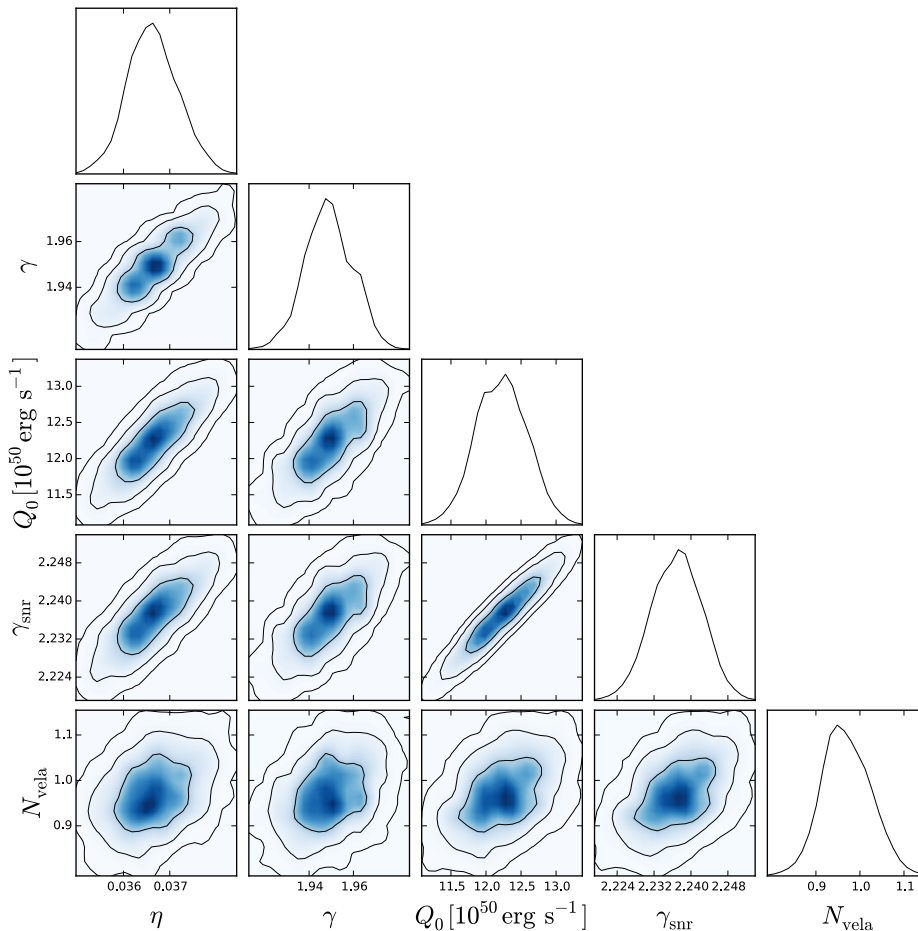


Figure 2. Triangular plot for the fit to AMS-02 data of the *astro model* parameters reported in Table 1. The contours refer to 1σ , 2σ and 3σ C.L. allowed regions. The plots along the diagonal show the posterior distribution for each parameter.

values for the normalization $Q_{0,\text{SNRs}}$ and the spectral index γ_{SNRs} of the injected electron flux. These parameters are left *free* to vary in our fitting procedure.

- Near SNRs ($d < 3$ kpc): the parameters that characterize these sources are derived directly from the Green catalogue [34], as anticipated in Section 2.2 and extensively discussed in Ref. [24]. Notice that, in order to allow for a better agreement with the electron flux at high energies, we introduce a free normalization for the Vela SNR, N_{Vela} , which therefore represents an additional parameter, not included in our previous analysis of Ref. [24]. Freedom in the variation of this parameter can be ascribed to variations in the value of the magnetic field of the source: $N_{\text{Vela}} \propto B^{-(\gamma_{\text{SNRs}}+1)/2}$, $N_{\text{Vela}} = 1$ corresponding to $B = 30 \mu\text{G}$.

- **Primary e^- and e^+ accelerated by PWNe:** by using the same approach of Ref. [24], we consider the PWNe of the ATNF catalog [44] as primary sources. The pulsars spin-down energies are derived from the catalog itself. The efficiency η_{PWNe} of conversion of this energy into electrons and positrons, and the spectral index γ_{PWNe} of the emission are assumed to be common to all the pulsars in the catalog and are free to vary.

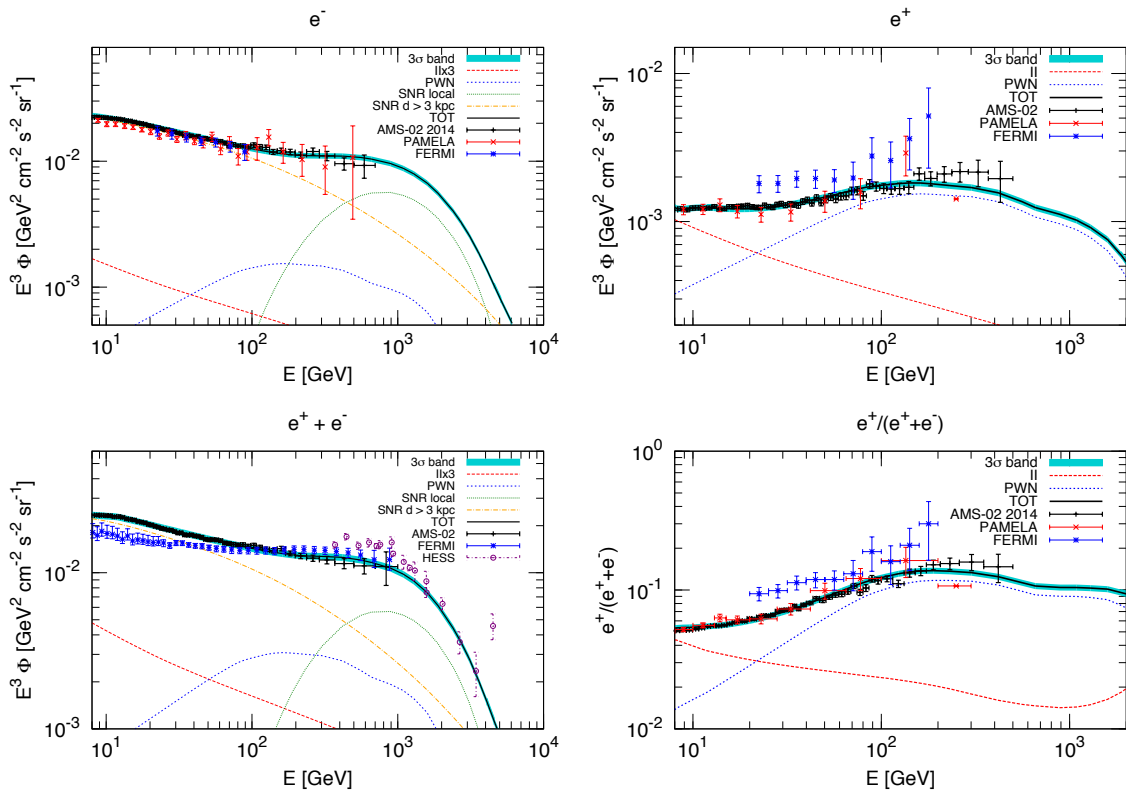


Figure 3. Astrophysical fit (*astro model*) to AMS-02 observables [53, 54, 57]. We display also Fermi-LAT [58, 59], PAMELA [60–62], and HESS data [29, 63]. The styles and colors used to represent the various contributions are described in the insets.

The contributions to the e^\pm fluxes coming from all these sources are propagated in the ISM and modulated in the heliosphere according to the prescriptions discussed in Section 3. While the reference model for the Galactic propagation is described by the MED set of parameters, the Fisk potential ϕ of the solar modulation is a free parameter.

To summarize, the *astro model* is characterized by six free parameters: $Q_{0,\text{SNRs}}$, γ_{SNRs} , N_{Vela} , η_{PWNe} , γ_{PWNe} and ϕ . Their best-fit values, together with their uncertainties, are reported in Table 1, while the triangular plot in Fig. 2 illustrates their posterior probability distributions, as they are sampled by the MCMC scan. Fig. 2 shows that the convergence of the sampling is good and the parameters are all well determined. From Table 1 we see that the average pulsars efficiency η_{PWNe} for the ATNF catalog sources is determined to be around 3.7%, a result well consistent with our previous findings [24], and that the Vela normalization preferred by the fit is close to the nominal value of our modeling ($N_{\text{Vela}} \sim 1$). The overall fit reproduces quite well the AMS-02 data, and has a reduced chi-square of 1.03, which translates into a p -value of 0.37, corresponding to a significance of the fit that is $\approx 1\sigma$.

Fig. 3 shows the comparison between the best-fit predictions of the *astro model* and AMS-02 data. As anticipated, the fluxes at lower energies are dominated by far SNRs in the case of electrons and by secondaries in the case of positrons, while local sources determine the fluxes in the high-energy window. This model predicts a relatively-flat, slightly-declining positron fraction for energies beyond the current AMS-02 measurements, up to at least the TeV range.

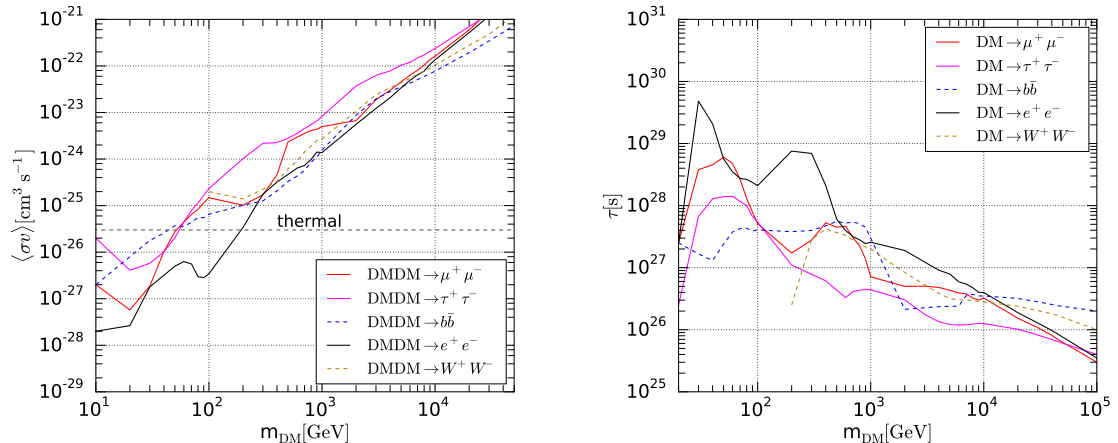


Figure 4. Constraints on the DM annihilation cross section $\langle\sigma v\rangle$ (left panel) and DM lifetime τ (right panel), for various production channels (as reported in the insets) in the *astro+DM model*. The constraints are computed at the 2σ C.L., and refer to the MED propagation model and Einasto DM density profile in our Galaxy.

The main conclusion that one can draw from this first part of our analysis, is similar to what we derived in Ref. [24]: the agreement between the *astro model* and the AMS-02 measurements is remarkably good and therefore a purely astrophysical interpretation of e^\pm data is perfectly viable. We also stress, as already found in Ref. [24], that the good agreement with the secondary positron flux in the low energy part of the positron spectrum is a hint in favor of a Galactic transport model close to the MED configuration, which refers to a CRs confinement region around 4 kpc.

4.2 Adding dark matter to the picture

The previous analysis for the *astro model* represents our baseline modeling, over which we now build the study of the information that can be derived on a DM contribution from the AMS-02 data. We therefore fit again the four experimental observables within a model that consists of all the primary and secondary astrophysical contributions discussed in the previous paragraph *plus* e^\pm fluxes produced by DM pair annihilation or decay. For definiteness, we refer to this modeling as the *astro+DM model*. The free parameters are now 8: the same $Q_{0,\text{SNRs}}$, γ_{SNRs} , N_{Vela} , η_{PWNe} , γ_{PWNe} , ϕ already introduced before, plus the two parameters characterizing the DM particle, namely its mass m_{DM} and annihilation cross-section $\langle\sigma v\rangle$ (or decay rate $\Gamma_{\text{dec}} = 1/\tau$).

Our investigation is twofold, being aimed at: *i*) deriving bounds on the DM annihilation/decay rate as a function of the DM mass (we will perform this analysis in a raster scan of the DM mass); *ii*) determining whether AMS-02 data require/prefer/allow a DM contribution. In both cases, our underlying assumption is that the DM contribution to the electron and positron fluxes occurs in the background of emission from astrophysical sources (SNRs and PWNe): this is likely the more plausible situation, and we wish to investigate whether, to what extent and how robustly a DM leptonic emission can be present in the CR fluxes. Our analysis will not restrict the DM contribution to be neither the dominant one, or the subdominant one a priori: we will just leave free the contribution from all sources (DM,

SNRs and PWNe) and adapt the modeling to the data with the same MCMC procedure discussed above.

4.2.1 Constraints on dark matter annihilation/decay

Let us move to the determination of upper bounds on the DM annihilation cross section $\langle\sigma v\rangle$ (or lower bounds on the decay lifetime τ) within a realistic full model for the astrophysical emission of primary and secondary e^\pm . We proceed as follows: for every DM annihilation/decay channel and for each value of the DM mass, we perform a MCMC sampling of the space defined by the 7 free parameters that characterize our model (6 astrophysical parameters plus $\langle\sigma v\rangle$ or τ). By marginalizing over the astrophysical-sources parameters, we derive the posterior distribution functions for the DM annihilation cross section (or lifetime, in case of decaying DM), from which 2σ C.L. upper limits are obtained. The results for both annihilating and decaying dark matter are shown in Fig. 4.

The bounds are quite constraining, especially in the low DM-mass region. For the annihilating case, the softer hadronic channels (here represented by the $b\bar{b}$ channel) exclude thermal annihilation cross section for DM masses below 40 GeV. The same occurs for the harder $\mu^+\mu^-$ and $\tau^+\tau^-$ channels, while for e^+e^- channel, which has the most prominent spectral feature [65], the bound on thermal cross sections increases at 200 GeV.

For the leptonic annihilation channels, we notice two features. The first is that for lighter DM, the bounds can be quite strong. Annihilation into leptons, especially the direct annihilation into a e^+e^- and to some extent also $\mu^+\mu^-$, have a hard energy spectrum with a characteristic feature [65], with a sharp fall-off: when the DM mass is below about 100 GeV, the feature occurs in the lower-energy portion of the positron flux, where the astrophysical contribution is dominated by the soft and smooth secondary flux which, as already mentioned, reproduces remarkably well the AMS-02 data. In this case, significantly strong bounds are obtained. The limits obtained here are on average in good agreement with the ones that have been derived in Refs. [22, 23], even though the astrophysical modeling in our analysis and in Refs. [22, 23] differ.

The second feature observable in the bounds of Fig. 4 for the e^+e^- and $\mu^+\mu^-$ channels is represented by a series of bumps that appear in the constraints. This corresponds to the fact that for some DM mass values, a contribution from DM annihilation or decay is actually preferred by the fit, and therefore the bounds weaken. These facts are investigated in the next Section.

4.2.2 Allowed regions in the DM parameters space

We therefore explicitly investigate which are the configurations in the DM parameters space that can provide the best fits to AMS-02 data. Instead of a raster scan on the DM mass, we investigate the full 8-fold parameter space of the *astro + DM model* in order to derive the best fit configurations together with their allowed regions. The results are reported in Table 2, while the triangular plot of Fig. 5 illustrates the posterior probability distributions of the parameters for the case in which DM annihilates into $\mu^+\mu^-$. The 1σ and 2σ contour plots in the $(m_{DM}, \langle\sigma v\rangle)$ plane for the annihilating DM case are reported in the upper row of Fig. 6 together with the bounds that have been found in Refs. [66, 67] as a result of an investigation of the different components contributing to the isotropic gamma-ray background (IGRB) measured by the *Fermi*-LAT experiment. Lastly, in the lower row of Fig. 6 the different contribution to the positron fraction measured by AMS-02 are shown for the best-fit configurations of the two cases of DM particles annihilating into the $\mu^+\mu^-$ and $b\bar{b}$ channels.

Annihilating DM					
Parameter	e^+e^-	$\mu^+\mu^-$	$\tau^+\tau^-$	$b\bar{b}$	W^+W^-
η_{PWNe}	$0.031^{+0.005}_{-0.001}$	$0.027^{+0.002}_{-0.002}$	$0.012^{+0.004}_{-0.001}$	$0.010^{+0.008}_{-0.009}$	$0.010^{+0.008}_{-0.009}$
γ_{PWNe}	$1.87^{+0.05}_{-0.03}$	$1.74^{+0.07}_{-0.13}$	$1.18^{+0.32}_{-0.18}$	$1.81^{+0.11}_{-0.25}$	$1.72^{+0.24}_{-0.21}$
$Q_{0,SNRs}[10^{50} \text{ erg/s}]$	$1.11^{+0.17}_{-0.06}$	$1.18^{+0.09}_{-0.11}$	$1.16^{+0.10}_{-0.07}$	$1.31^{+0.08}_{-0.10}$	$1.26^{+0.10}_{-0.08}$
γ_{SNRs}	$2.22^{+0.03}_{-0.01}$	$2.23^{+0.01}_{-0.02}$	$2.23^{+0.02}_{-0.01}$	$2.25^{+0.01}_{-0.01}$	$2.24^{+0.01}_{-0.01}$
N_{Vela}	$0.87^{+0.16}_{-0.16}$	$0.81^{+0.16}_{-0.17}$	$0.99^{+0.10}_{-0.25}$	$0.89^{+0.15}_{-0.15}$	$0.88^{+0.16}_{-0.15}$
$m_{DM} [\text{GeV}]$	51^{+1}_{-18}	89^{+22}_{-10}	619^{+76}_{-211}	39000^{+11010}_{-25100}	17400^{+29700}_{-8150}
$\langle\sigma v\rangle [\text{cm}^3\text{s}^{-1}]$	$5.2^{+1.4}_{-3.8} \times 10^{-27}$	$8.4^{+7.7}_{-3.0} \times 10^{-26}$	$6.8^{+1.4}_{-3.3} \times 10^{-24}$	$7.7^{+3.6}_{-6.1} \times 10^{-22}$	$3.5^{+10.9}_{-2.2} \times 10^{-22}$
$\chi^2/\text{d.o.f.}$	0.91	0.78	0.84	0.95	0.95
$p\text{-value}(\text{sign.})$	0.20(1.3 σ)	1.1×10^{-2} (2.5 σ)	5.8×10^{-2} (1.9 σ)	0.33(1.0 σ)	0.31(1.0 σ)
Decaying DM					
Observable	e^+e^-	$\mu^+\mu^-$	$\tau^+\tau^-$	$b\bar{b}$	W^+W^-
η_{PWNe}	$0.031^{+0.003}_{-0.001}$	$0.026^{+0.003}_{-0.001}$	$0.012^{+0.004}_{-0.002}$	$0.010^{+0.088}_{-0.001}$	$0.011^{+0.006}_{-0.001}$
γ_{PWNe}	$1.87^{+0.05}_{-0.04}$	$1.69^{+0.12}_{-0.08}$	$1.14^{+0.03}_{-0.02}$	$1.78^{+0.14}_{-0.22}$	$1.72^{+0.15}_{-0.22}$
$Q_{0,SNRs}[10^{50} \text{ erg/s}]$	$1.09^{+0.18}_{-0.06}$	$1.14^{+0.12}_{-0.07}$	$1.15^{+0.10}_{-0.06}$	$1.29^{+0.10}_{-0.08}$	$1.27^{+0.09}_{-0.08}$
γ_{SNRs}	$2.22^{+0.02}_{-0.01}$	$2.22^{+0.02}_{-0.01}$	$2.227^{+0.015}_{-0.011}$	$2.25^{+0.01}_{-0.01}$	$2.24^{+0.01}_{-0.01}$
N_{Vela}	$0.85^{+0.16}_{-0.11}$	$0.75^{+0.19}_{-0.13}$	$0.91^{+0.18}_{-0.15}$	$0.86^{+0.19}_{-0.11}$	$0.90^{+0.13}_{-0.17}$
$m_{DM} [\text{GeV}]$	99^{+6}_{-33}	194^{+16}_{-32}	1210^{+180}_{-390}	78200^{+21800}_{-49600}	35800^{+14200}_{-17100}
$\tau [\text{s}]$	$2.6^{+3.5}_{-0.6} \times 10^{28}$	$2.2^{+1.2}_{-0.4} \times 10^{27}$	$2.4^{+0.6}_{-0.2} \times 10^{26}$	$1.3^{+13}_{-1.0} \times 10^{26}$	$1.19^{+1.71}_{-0.15} \times 10^{26}$
$\chi^2/\text{d.o.f.}$	0.92	0.80	0.84	0.95	0.92
$p\text{-value}(\text{sign.})$	0.21(1.2 σ)	2.3×10^{-2} (2.2 σ)	5.2×10^{-2} (1.9 σ)	0.33(1.0 σ)	0.24(1.2 σ)

Table 2. Best-fit configurations for the *astro+DM* model.

As it can be clearly seen, the fitting procedure can reach a very high resolution in determining the mass and the annihilation cross section/lifetime for the leptonic annihilation/decay channels. This is a consequence of the fact that these channels are expected to produce sharply peaked positron spectra which basically contribute to replenish the gap at intermediate energies (*i.e.* between 20 and 40 GeV), where the secondary flux begins to become negligible and the contribution from PWNe starts getting relevant. In this relatively small energy window, small variations in DM parameters can lead to large fluctuations of the chi-square and this makes the contour regions in the $(m_{DM}, \langle\sigma v\rangle)$ plane quite small. A different situation occurs for hadronic channels, for which the DM contribution extends over several energy bins, from intermediate energies up to the last AMS-02 bins: in a large fraction of this energy range, the contribution from DM is degenerate with the contribution from PWNe and thus quite large variations in DM properties do not always translate into large fluctuations on the chi-square.

Concerning the comparison with gamma-ray constraints on the same annihilation channels, the upper row of Fig. 6 reports the upper limits on the DM thermally averaged annihilation cross section $\langle\sigma v\rangle$ computed in Refs. [66, 67] by means of a detail modelling of the various contribution to the IGRB energy spectrum that can be derived from the measurements performed by the *Fermi*-LAT experiment. In particular, solid lines represent *conservative* upper limits as reported in Ref. [66] with the γ -ray emission from extragalactic sources set to the minimal level allowed in their modeling, while dashed lines refer to *optimistic* upper limits

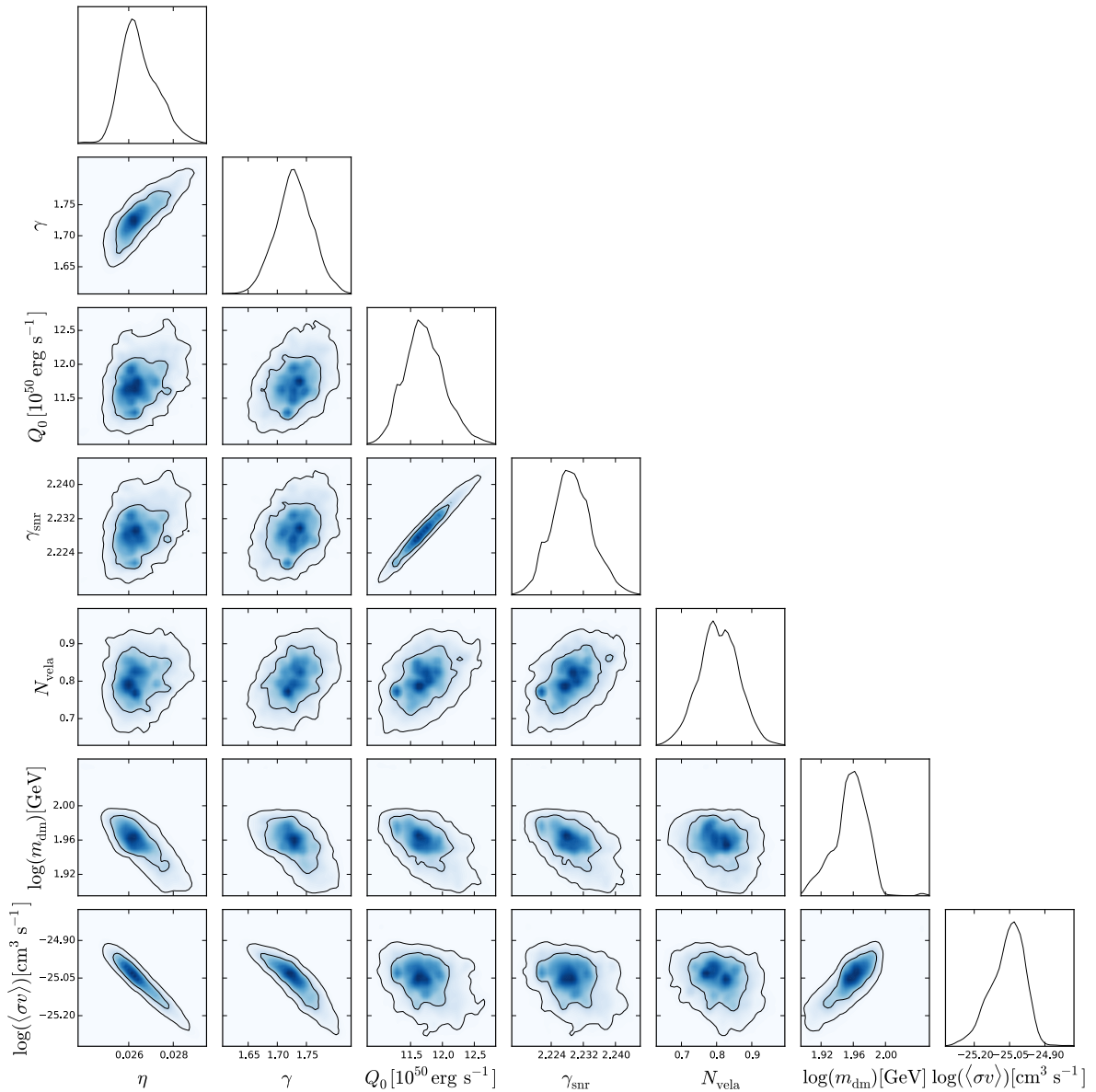


Figure 5. Triangular plot for the fit of the parameters of the *astro+DM* model to AMS-02 data, for a DM annihilating into the $\mu^+\mu^-$ channel. The contours refer to 1σ , 2σ and 3σ C.L. allowed regions. The plots along the diagonal show the posterior distribution for each parameter.

derived in Ref. [67] from a statistical fit to the *Fermi*-LAT IGRB data. As it can be seen, only the annihilation in the e^+e^- and $\mu^+\mu^-$ channels is fully consistent with the gamma-ray bounds, while for all the other channels a tension is present, even in a conservative setup.

The last result worth emphasizing is that the values of the chi-square that characterize the fits for the different annihilation/decay channels are quite good, especially for the $\mu^+\mu^-$ and $\tau^+\tau^-$ channels, definitely better than the one obtained for the pure *astro* model. In other words, for these channels, adding a DM contribution to the e^\pm astrophysical emission sizeably improves the agreement with the AMS-02 data, decreasing the p -value of the fit from 0.45 (about 1σ) for the pure astrophysical interpretation to 6×10^{-3} (2.7σ) for the $\mu^+\mu^-$

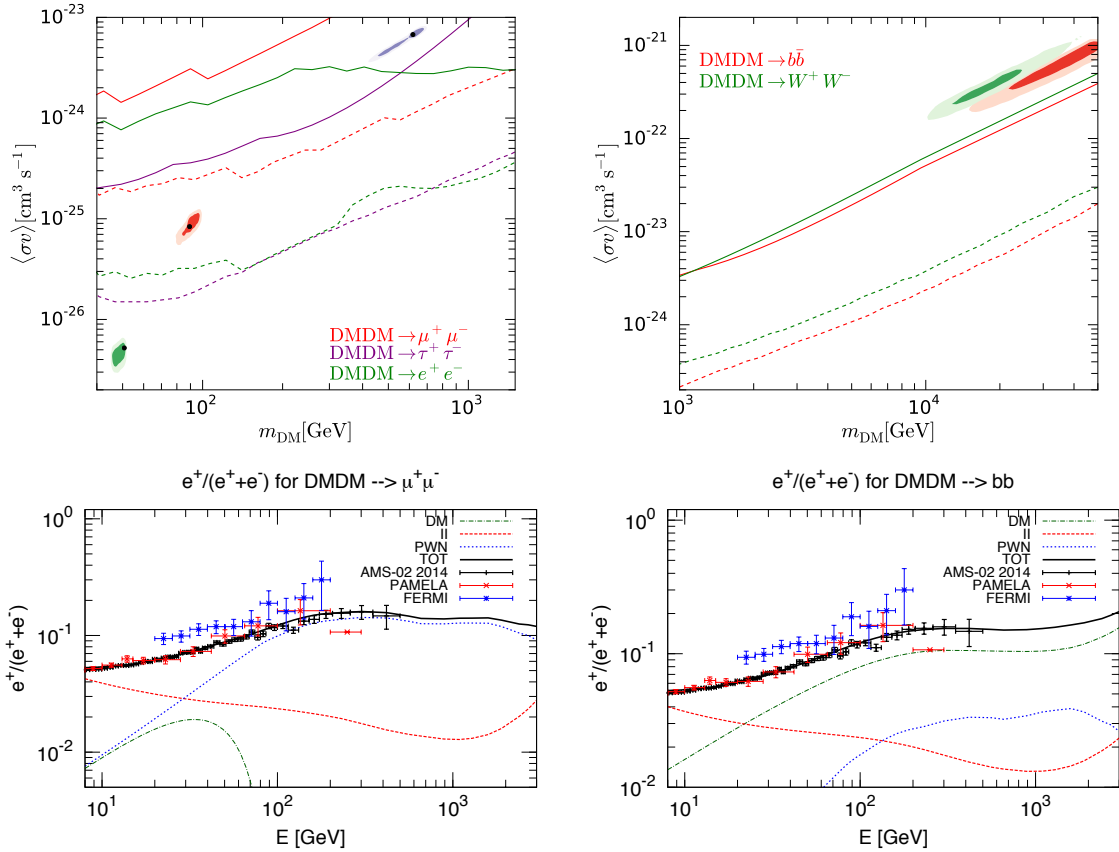


Figure 6. Upper row: allowed regions in the $(m_{DM}, \langle\sigma v\rangle)$ for a DM particle annihilating into leptonic (*left panel*) or hadronic (*right panel*) channels. For every channel, the different shadings correspond to the 1σ and 2σ contour regions, while the solid and dashed lines represent, respectively, the conservative and optimistic gamma-ray upper limits derived in Refs. [66, 67]. In the lower row, the contributions to the positron fraction associated to the best-fit configurations for a DM annihilating in $\mu^+ \mu^-$ (*left panel*) and $b\bar{b}$ (*right panel*) are shown.

channel, as can be seen by comparing the results in Table 1 and Table 2. We notice that also for the *astro+DM* model, the positron fraction keeps a flat behaviour beyond the current AMS-02 data: this is a consequence of the fact that the addition of a DM component is driven to contribute to intermediate energies, and leaves the high-energy part of the positron spectrum basically unchanged from the pure astrophysical interpretation.

4.2.3 Varying the astrophysical modeling

In this Section we explore the consequences of relaxing some of the assumptions that, in the previous Sections, have been made about the contribution from PWNe. This should allow us to understand to what extent the remarkable agreement that we have found in the *astro+DM model* can be interpreted as a genuine hint of DM, capable of surviving even within a more complex modeling of the PWNe contribution.

As a first analysis, we carry out a simple exercise to assess what would be the properties of a putative pulsar that, added to the ones of the ATNF catalogue, would be able to provide an agreement to AMS-02 data as good as the one obtained with the addition of DM. We are

Parameter	central value $\pm 1\sigma$
η_{PWNe}	$0.06^{+0.04}_{-0.01}$
γ_{PWNe}	$1.4^{+0.2}_{-0.1}$
$Q_{0,SNRs} [10^{50} \text{ erg/s}]$	$1.13^{+0.05}_{-0.05}$
γ_{SNRs}	$2.22^{+0.01}_{-0.01}$
N_{Vela}	$0.9^{+0.1}_{-0.2}$
$d_{psr} [\text{kpc}]$	$0.59^{+0.11}_{-0.15}$
$T_{psr} [\text{kyr}]$	980^{+820}_{-210}
η_{psr}	$0.45^{+0.07}_{-0.13}$
$\chi^2/\text{d.o.f.} = 0.70$ and $p\text{-value} = 6.8 \times 10^{-4}$ (3.4σ)	

Table 3. Best fit for the *astro model* with an additional PWN. For every parameter the best-fit value is reported together with the upper and lower 1σ uncertainty. The value of η_{psr} has been derived assuming a spin-down luminosity for the additional PWN equal to $\dot{E} = 10^{34}$ erg/s, for definiteness.

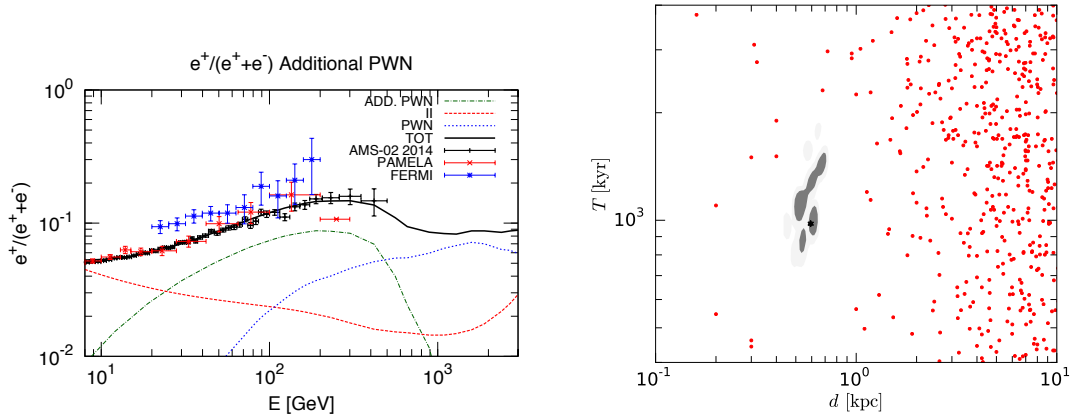


Figure 7. The *left panel* shows the contribution of the additional PWN to the positron fraction. The *right panel* reports the contour plot of the distance and age of the additional pulsar together with the other sources from the ATNF catalogue; the star denotes the best-fit, while the darker and lighter shadings represent, respectively, the 1σ and 2σ confidence regions.

therefore trying to replace the DM electron-positron production with a generic additional PWN emission, to see if this can fully mimic a DM contributions and what are the properties required for such a pulsar. To this aim, we perform a fit to AMS-02 data within a version of the *astro model*, modified in such a way to include an additional PWN, whose distance d_{psr} , age T_{psr} and total energy emitted in the form of e^\pm pairs $\eta_{psr}W_{0,psr}$ are to be determined by a fit to the data. This brings the total number of free parameters in our fit to 9: $Q_{0,SNRs}$, γ_{SNRs} , N_{Vela} , η_{PWNe} , γ_{PWNe} , ϕ , d_{psr} , T_{psr} and $\eta_{psr}W_{0,psr}$.

The result of the fit is shown in Table 3, while the best-fit configuration and the 1σ and 2σ C.L. regions for the additional pulsar in the (d_{psr}, T_{psr}) plane are reported together with the PWNe listed in the ATNF catalogue in the left panel of Fig. 7. The right panel shows instead the predicted positron fraction for the best-fit configuration, together with the AMS-

Annihilating DM				
Parameter	astro	e^+e^-	$\mu^+\mu^-$	$\tau^+\tau^-$
η_{PWNe}	$14.9^{+52.1}_{-4.0} \times 10^{-4}$	$6.7^{+67.9}_{-5.7} \times 10^{-4}$	$36.2^{+14.2}_{-21.8} \times 10^{-4}$	$6.5^{+65.5}_{-6.4} \times 10^{-4}$
γ_{PWNe}	$1.41^{+1.00}_{-0.01}$	$1.95^{+0.25}_{-0.50}$	$1.83^{+0.07}_{-0.14}$	$1.64^{+0.56}_{-0.19}$
η_1	$0.112^{+0.026}_{-0.061}$	$0.095^{+0.027}_{-0.081}$	$0.027^{+0.020}_{-0.003}$	$0.105^{+0.035}_{-0.063}$
η_2	$0.005^{+0.027}_{-0.004}$	$0.004^{+0.026}_{-0.001}$	$0.004^{+0.009}_{-0.003}$	$0.003^{+0.029}_{-0.003}$
η_3	$0.025^{+0.089}_{-0.024}$	$0.049^{+0.062}_{-0.048}$	$0.011^{+0.013}_{-0.010}$	$0.062^{+0.082}_{-0.061}$
η_4	$0.258^{+0.049}_{-0.093}$	$0.300^{+0.056}_{-0.135}$	$0.445^{+0.015}_{-0.045}$	$0.279^{+0.076}_{-0.134}$
η_5	$0.016^{+0.110}_{-0.006}$	$0.016^{+0.192}_{-0.015}$	$0.034^{+0.003}_{-0.024}$	$0.003^{+0.136}_{-0.003}$
$Q_{0,SNRs} [10^{50} \text{ erg/s}]$	$1.14^{+0.11}_{-0.05}$	$1.14^{+0.07}_{-0.06}$	$1.12^{+0.03}_{-0.02}$	$1.15^{+0.13}_{-0.05}$
γ_{SNRs}	$2.22^{+0.02}_{-0.01}$	$2.22^{+0.01}_{-0.01}$	$2.22^{+0.01}_{-0.01}$	$2.23^{+0.01}_{-0.01}$
N_{Vela}	$0.85^{+0.15}_{-0.17}$	$0.79^{+0.21}_{-0.15}$	$0.80^{+0.04}_{-0.04}$	$0.78^{+0.21}_{-0.12}$
$m_{DM} [\text{GeV}]$	-	31^{+53}_{-10}	51^{+10}_{-3}	140^{+7}_{-7}
$\langle \sigma v \rangle [\text{cm}^3 \text{s}^{-1}]$	-	1.08×10^{-27}	$2.8^{+1.1}_{-0.5} \times 10^{-26}$	$4.3^{+16.0}_{-4.2} \times 10^{-26}$
$\chi^2/\text{d.o.f.}$	0.80	0.78	0.67	0.75
$p\text{-value}(\text{sign.})$	$2.2 \times 10^{-2} (2.2\sigma)$	$1.2 \times 10^{-2} (2.5\sigma)$	$2.7 \times 10^{-4} (3.6\sigma)$	$4.8 \times 10^{-3} (2.8\sigma)$

Table 4. Best-fit configurations for the *refined astro model*.

02 data. The “fictitious” pulsar that we are adding sizably improves the agreement with the AMS-02 data as compared to the *astro model* and provides a fit that is comparable to the ones that are associated to a DM signal in the muon channel, as reported in Table 2. This occurs if this source is able to provide a non-negligible contribution in the low/intermediate-energy region of the positron flux, which, as already stressed, is where also the DM contribution from leptonic annihilation/decay channels was preferred by the fit. In order to have a sizeable flux at these energies, the pulsar should be relatively close (600 pc), young (1000 kyr) and powerful ($\eta_{\text{psr}} W_0 = 1.4^{+0.2}_{-0.4} \times 10^{39}$ erg). From Fig. 7 we see that the ATNF catalogue does not contain PWN in the region preferred by the fit to the AMS-02 data.

Notice that the addition of a “fictitious” PWN could have, in principle, led to a solution close to a source with age and distance similar to those belonging to one of the pulsars in the ATNF catalogue: in fact, for this putative source we let free also the parameter η_{psr} that controls the energetics of its emission in the electron-positron channel, while instead for all the PWN contained in the ATNF catalogue we assume the same η_{PWNe} , as a common average value. If we had found that the “fictitious” pulsars lied close to one of the ATNF catalogue, this would have implied that that specific catalogue-pulsar would have required an increased emission power $(\eta W_0)_{\text{PWNe}} + (\eta W_0)_{\text{psr}}$. Since the solution falls in a region where the ATNF catalogue has no sources could mean that: *i*) the DM interpretation is preferred; *ii*) if that additional pulsar exists, it must produce a detectable flux of electron and positron, while at the same time being able to evade other observations in the multiwavelength bands (an investigation along this lines is beyond the scope of this paper).

As a second extension of the analysis of the previous Sections, and in order to investigate at a deeper level what we can do with the sources that are in the ATNF catalogue, we build a more complex astrophysical framework, which we label *refined astro model*, that is characterized by the assumption that the whole set of PWNe listed in the ATNF catalogue do not share anymore the same efficiency η_{PWNe} . Instead, we single out the five most powerful

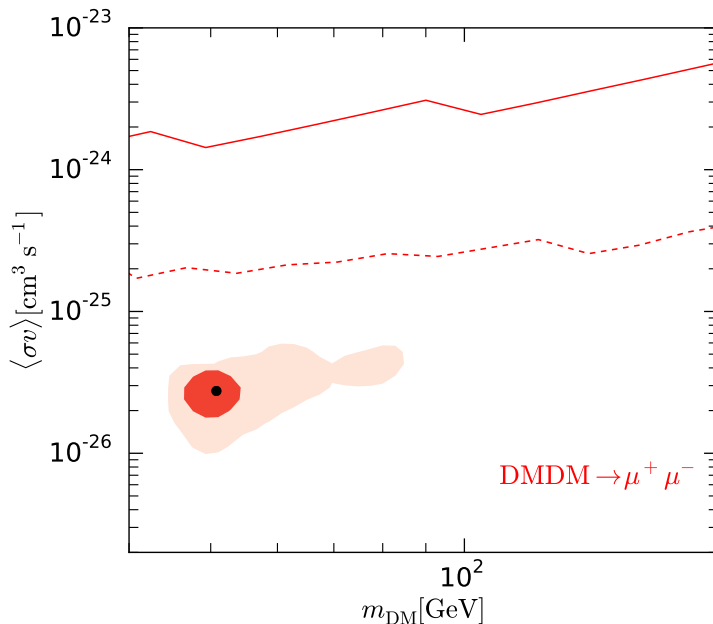


Figure 8. 1σ and 2σ allowed regions in the $(m_{DM}, \langle\sigma v\rangle)$ plane for a DM annihilating in the $\mu^+\mu^-$ channel in the *refined astro model with DM*. Solid and dashed lines represent, respectively, the conservative and optimistic gamma-ray upper limits derived in Refs. [66, 67].

sources of the catalogue in the different energy ranges by using the same ranking algorithm that has been used in Ref. [24] and we associate to their emissions the efficiencies η_i (being $i = 1, \dots, 5$) that act as free parameters in our fitting procedure. These most powerful sources are [24]: Geminga ($i = 1$), J2043+2740 ($i = 2$), J0538+2817 ($i = 3$), Monogem ($i = 4$) and B1742-30 ($i = 5$). To limit the number of parameters in the fit we associate to each one of these five sources the same spectral index $\gamma_{i=1,\dots,5} = 1.8$ [24] (we have checked that different values for this parameter does not affect our conclusions). The parameters η_{PWNe} and γ_{PWNe} , whose definition has been given in the previous Sections, are still present and characterize the population of the *other* PWNe in the ATNF catalogues, which behave like a background of sources that share common values for their efficiencies and spectral indices. To summarize: we consider emission from the full ATNF catalogue, but for the 5 most powerful sources we allow for a free normalization parameter on their emission.

In Table 4 we list the best-fit configurations that are obtained by fitting AMS-02 data within the *refined astro model*, *without* and *with* the addition of DM. We illustrate only the results obtained for the annihilating case, since we do not register any significant change for a DM that decays in the same channels (except for the fact that the best-fit DM masses are halved). We show only the best-fit configurations for the leptonic channels, since for DM annihilation into the $b\bar{b}$ and W^+W^- channels the addition of a DM signal does not improve the fit as compared to the purely astrophysical case.

In the case of a pure astrophysical interpretation, the results in terms of the reconstructed parameters are stable as compared to the ones obtained in the *astro model*, with the notable exception of the emission coefficient η_i for the 5 most powerful PWN: Geminga and Monogem are required to be the dominant emitters. The catalogue-PWN other than the 5

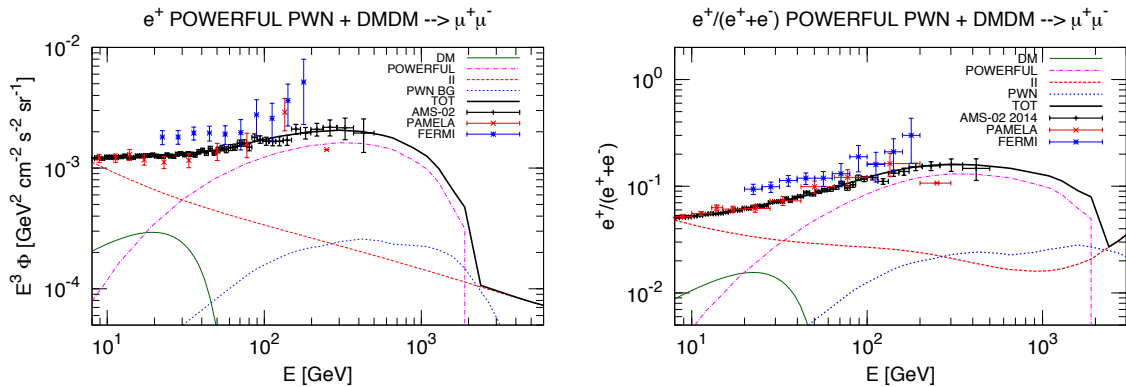


Figure 9. In the left (right) panel the contributions to the positron (positron fraction) associated to the best-fit configuration for a DM annihilating in $\mu^+\mu^-$ channel (solid green line), with the flux from the five most powerful sources (dot-dashed magenta line), from all the other pulsars of the ATNF catalog (dotted blue line) and from secondary production (dashed red line) are shown.

most powerful are now significantly suppressed as compared to the previous analysis of the *astro model*: η_{PWN_e} drops from 3.6% to 0.1%. This implies that the AMS-02 data could be shaped by very few dominant sources, like Monogem and Geminga. The significance of the fit is here improved as compared to the simpler *astro model*.

In the case a DM signal is present, we see that also within this more complex model for the astrophysical emission, the contribution from a DM annihilating into leptons is able to sizably improve the fit to AMS-02 data: in particular, for the annihilation into $\mu^+\mu^-$ and $\tau^+\tau^-$, the significance is definitely higher than in the *astro+DM model*: the p -values of the best fits improve from 1.1×10^{-2} (significance of 2.5σ) to 2.7×10^{-4} (3.6σ) for the $\mu^+\mu^-$ channel and from 5.8×10^{-2} (1.9σ) to 4.8×10^{-3} (2.8σ) for the $\tau^+\tau^-$ channel. The $\tau^+\tau^-$ case is still in tension with the γ -ray constraints shown in Fig. 6, while the $\mu^+\mu^-$ DM candidate is fully compatible with these bounds, and therefore represent the best option for a DM interpretation. In the case of the preferred $\mu^+\mu^-$ channel, the best-fit mass in the *refined astro model* turns out to be somehow smaller as compared to the *astro model* (51 GeV instead of 89 GeV) and the annihilation cross section is about a factor of four smaller, being compatible with the thermal value at the 2σ level. The allowed region and the gamma-rays bounds for the $\mu^+\mu^-$ channel are shown in Fig. 8. We wish to stress that the $\Delta\chi^2$, namely the difference of the chi-square considering the refined purely-astrophysical model and the model with the addition of DM annihilating into $\mu^+\mu^-$ is 24, therefore the p -value for the addition of this exotic contribution is 6.1×10^{-6} associated to a significance of the preference of DM in our model of about 4.5σ . Therefore in the contest of our astrophysical model the DM contribution with a $\mu^+\mu^-$ annihilation channel is significantly preferred and is fully consistent with γ -ray bounds, and with constraints arising from the CMB [68, 69]. We notice also that in this case, Monogem is the largely dominant pulsar emitter.

The spectral features of the best fit results for the *refined astro model with DM*, which occurs for the $\mu^+\mu^-$ channel, are shown in Fig. 9: the positron flux in the left panel, the positron fraction in the right panel. Notice that in this case, where a single pulsar largely dominates the positron flux (Monogem), the positron fraction is predicted to drop relatively quickly at the pulsars cut-off energy (which in our analysis is taken at 2 TeV). This feature is here due not to the DM emission (which, in this case, gives its maximal contribution at

intermediate energies), but to the pulsars high energy properties. Data above the TeV scale could help in distinguishing the situation where all known pulsars contribute in a democratic way (*astro model*, with or without DM), from a case where a single pulsar dominates the high-energy positron emission (in our analysis, the *refined astro model*, again with or without a DM contribution).

5 Conclusions

In this paper we have performed a quantitative study of AMS-02 electron and positron data, in terms of both galactic known sources and a possible dark matter contribution. Firstly, by updating the analysis illustrated in Ref. [24], we have investigated the possibility to interpret the whole set of leptonic AMS-02 data in terms of astrophysical sources of primary and secondary origin only. We have shown that even under few simplifying assumptions, *i.e.* assuming the same efficiency and spectral index for all the PWNe of the ATNF catalogue, our model can provide a rather good fit to all the data. Secondly, we have carried out a detailed study of the interplay between the contributions to the positron flux that derive from primary astrophysical sources (namely PWNe) and from the annihilation/decay of DM particles. We have worked within a scenario in which DM gives its contribution on top of a realistic astrophysical leptonic emission, which acts as a non trivial background with respect to a putative DM signal. On one hand, we have investigated how one can use the highly precise data provided by the AMS-02 experiment to derive robust constraints to DM properties. On the other hand, we have illustrated how the addition of a DM contribution compatible with the bounds that arise from other indirect detection channels, can improve the fit to AMS-02 data. Specifically, we have found that a DM particle with a mass around 50 GeV, annihilating in the $\mu^+\mu^-$ channel with a cross section remarkably close to the thermal value can provide, when added to the PWNe and to the secondary contributions, an excellent fit to the AMS-02 data, significantly better than adopting a purely astrophysical positron emission. Conversely, the addition of a DM annihilating or decaying into hadronic channels, does not appear to improve the fit significantly and the best-fit configurations for these channels are in tension with upper bounds derived from different indirect DM searches (e.g. gamma-rays).

We have also investigated whether the addition of a local pulsar to sources of the ATNF catalogue can provide a fit to the AMS-02 data of comparable goodness as the DM hypothesis. This is indeed possible, although the characteristics (distance and age) of this additional pulsar do not correspond to any source already present in the ATNF catalogue. Therefore this interpretation seems to be either worse than the DM hypothesis or to imply specific characteristics for the additional pulsar, like detectable production of e^\pm accompanied by a reduced (currently unobservable) emission in electromagnetic channels.

We conclude by saying that the parallel inspection of independent and multi-wavelength channels is a crucial step in pursuing a deeper understanding of the astrophysical sources that populate our Galactic environment. This investigation, together with the precise measurements performed by current and future experiments may significantly help in interpreting the cosmic lepton data and, perhaps, in shedding light on the DM mystery.

Acknowledgments

This work is supported by the research grant *Theoretical Astroparticle Physics* number 2012CPPYP7, funded under the program PRIN 2012 of the Ministero dell’Istruzione, Univer-

sità e della Ricerca (MIUR), by the research grant *TAsP (Theoretical Astroparticle Physics)* funded by the Istituto Nazionale di Fisica Nucleare (INFN), and by the *Strategic Research Grant: Origin and Detection of Galactic and ExtraGalactic Cosmic Rays* funded by Torino University and Compagnia di San Paolo. A.V acknowledges the hospitality of the IPhT CEA Saclay and of the Institut d’Astrophysique de Paris (IAP) where part of this work was done.

References

- [1] **PAMELA** Collaboration, O. Adriani et al., *An anomalous positron abundance in cosmic rays with energies 1.5-100 GeV*, *Nature* **458** (2009) 607–609, [[arXiv:0810.4995](#)].
- [2] L. Bergstrom, T. Bringmann, and J. Edsjo, *New Positron Spectral Features from Supersymmetric Dark Matter - a Way to Explain the PAMELA Data?*, *Phys.Rev.* **D78** (2008) 103520, [[arXiv:0808.3725](#)].
- [3] I. Cholis, L. Goodenough, D. Hooper, M. Simet, and N. Weiner, *High Energy Positrons From Annihilating Dark Matter*, *Phys.Rev.* **D80** (2009) 123511, [[arXiv:0809.1683](#)].
- [4] M. Cirelli, M. Kadastik, M. Raidal, and A. Strumia, *Model-independent implications of the e^+ , anti-proton cosmic ray spectra on properties of Dark Matter*, *Nucl.Phys.* **B813** (2009) 1–21, [[arXiv:0809.2409](#)].
- [5] G. Bertone, M. Cirelli, A. Strumia, and M. Taoso, *Gamma-ray and radio tests of the e^+e^- excess from DM annihilations*, *JCAP* **0903** (2009) 009, [[arXiv:0811.3744](#)].
- [6] E. Nardi, F. Sannino, and A. Strumia, *Decaying Dark Matter can explain the e^+e^- excesses*, *JCAP* **0901** (2009) 043, [[arXiv:0811.4153](#)].
- [7] D. Hooper, A. Stebbins, and K. M. Zurek, *Excesses in cosmic ray positron and electron spectra from a nearby clump of neutralino dark matter*, *Phys.Rev.* **D79** (2009) 103513, [[arXiv:0812.3202](#)].
- [8] D. Hooper and K. M. Zurek, *The PAMELA and ATIC Signals From Kaluza-Klein Dark Matter*, *Phys.Rev.* **D79** (2009) 103529, [[arXiv:0902.0593](#)].
- [9] D. Hooper, P. Blasi, and P. D. Serpico, *Pulsars as the Sources of High Energy Cosmic Ray Positrons*, *JCAP* **0901** (2009) 025, [[arXiv:0810.1527](#)].
- [10] H. Yuksel, M. D. Kistler, and T. Stanev, *TeV Gamma Rays from Geminga and the Origin of the GeV Positron Excess*, *Phys.Rev.Lett.* **103** (2009) 051101, [[arXiv:0810.2784](#)].
- [11] S. Profumo, *Dissecting cosmic-ray electron-positron data with Occam’s Razor: the role of known Pulsars*, *Central Eur.J.Phys.* **10** (2011) 1–31, [[arXiv:0812.4457](#)].
- [12] Y. Fujita, K. Kohri, R. Yamazaki, K. Ioka, K. Kohri, et al., *Is the PAMELA anomaly caused by the supernova explosions near the Earth?*, *Phys.Rev.* **D80** (2009) 063003, [[arXiv:0903.5298](#)].
- [13] P. Blasi, *The origin of the positron excess in cosmic rays*, *Phys. Rev. Lett.* **103** (2009) 051104, [[arXiv:0903.2794](#)].
- [14] M. Ahlers, P. Mertsch, and S. Sarkar, *Cosmic ray acceleration in supernova remnants and the fermi/pamela data*, *Phys. Rev. D* **80** (Dec, 2009) 123017.
- [15] J. Lavalle, D. Maurin, and A. Putze, *Direct constraints on diffusion models from cosmic-ray positron data: Excluding the minimal model for dark matter searches*, *Phys. Rev.* **D90** (2014) 081301, [[arXiv:1407.2540](#)].
- [16] M. Boudaud et al., *A new look at the cosmic ray positron fraction*, *Astron. Astrophys.* **575** (2015) A67, [[arXiv:1410.3799](#)].
- [17] P. Mertsch and S. Sarkar, *AMS-02 data confront acceleration of cosmic ray secondaries in nearby sources*, *Phys. Rev.* **D90** (2014) 061301, [[arXiv:1402.0855](#)].

- [18] S.-J. Lin, Q. Yuan, and X.-J. Bi, *Quantitative study of the AMS-02 electron/positron spectra: Implications for pulsars and dark matter properties*, *Phys. Rev.* **D91** (2015), no. 6 063508, [[arXiv:1409.6248](#)].
- [19] H.-B. Jin, Y.-L. Wu, and Y.-F. Zhou, *Cosmic ray propagation and dark matter in light of the latest AMS-02 data*, [arXiv:1410.0171](#).
- [20] T. Delahaye, K. Kotera, and J. Silk, *What could we learn from a sharply falling positron fraction?*, *Astrophys. J.* **794** (2014), no. 2 168, [[arXiv:1404.7546](#)].
- [21] D. Gaggero, L. Maccione, D. Grasso, G. Di Bernardo, and C. Evoli, *PAMELA and AMS-02 e^+ and e^- spectra are reproduced by three-dimensional cosmic-ray modeling*, *Phys. Rev.* **D89** (2014) 083007, [[arXiv:1311.5575](#)].
- [22] A. Ibarra, A. S. Lamperstorfer, and J. Silk, *Dark matter annihilations and decays after the AMS-02 positron measurements*, *Phys.Rev.* **D89** (2014), no. 6 063539, [[arXiv:1309.2570](#)].
- [23] L. Bergstrom, T. Bringmann, I. Cholis, D. Hooper, and C. Weniger, *New limits on dark matter annihilation from AMS cosmic ray positron data*, *Phys.Rev.Lett.* **111** (2013) 171101, [[arXiv:1306.3983](#)].
- [24] M. Di Mauro, F. Donato, N. Fornengo, R. Lineros, and A. Vittino, *Interpretation of AMS-02 electrons and positrons data*, *JCAP* **1404** (2014) 006, [[arXiv:1402.0321](#)].
- [25] **AMS** Collaboration, M. Aguilar et al., *Precision Measurement of the Proton Flux in Primary Cosmic Rays from Rigidity 1 GV to 1.8 TV with the Alpha Magnetic Spectrometer on the International Space Station*, *Phys. Rev. Lett.* **114** (2015), no. 17 171103.
- [26] AMS-02 Collaboration, “Talks at the ams days at cern, 15-17 april 2015.” <http://indico.cern.ch/event/381134/>.
- [27] T. Kamae, N. Karlsson, T. Mizuno, T. Abe, and T. Koi, *Parameterization of γ , $e^{+/-}$, and Neutrino Spectra Produced by p - p Interaction in Astronomical Environments*, *ApJ* **647** (Aug., 2006) 692–708, [[astro-ph/0605581](#)].
- [28] J. W. Norbury and L. W. Townsend, *Parameterized total cross sections for pion production in nuclear collisions*, *Nuclear Instruments and Methods in Physics Research B* **254** (Jan., 2007) 187–192, [[nucl-th/0612081](#)].
- [29] F. Aharonian, A. G. Akhperjanian, et al., *Energy Spectrum of Cosmic-Ray Electrons at TeV Energies*, *Phys.Rev.Lett.* **101** (Dec., 2008) 261104, [[arXiv:0811.3894](#)].
- [30] F. Aharonian, A. G. Akhperjanian, U. B. de Almeida, et al., *Discovery of Gamma-Ray Emission From the Shell-Type Supernova Remnant RCW 86 With HESS*, *ApJ* **692** (Feb., 2009) 1500–1505, [[arXiv:0810.2689](#)].
- [31] **VERITAS** Collaboration, V. A. Acciari et al., *Observations of the Shell-type Supernova Remnant Cassiopeia A at TeV Energies with VERITAS*, *ApJ* **714** (May, 2010) 163–169, [[arXiv:1002.2974](#)].
- [32] **HEGRA** Collaboration, F. Aharonian, *Evidence for TeV gamma-ray emission from cassiopeia a*, *A&A* **370** (2001) 112–120, [[astro-ph/0102391](#)].
- [33] Aharonian et al., *Primary particle acceleration above 100 TeV in the shell-type supernova remnant RX J1713.7-3946 with deep HESS observations*, *A&A* **464** (Mar., 2007) 235–243, [[astro-ph/0611813](#)].
- [34] D. Green, *A catalogue of 294 Galactic supernova remnants*, *Bull.Astron.Soc.India* **42** (2014) 47, [[arXiv:1409.0637](#)].
- [35] C. S. Shen, *Pulsars and Very High-Energy Cosmic-Ray Electrons*, *ApJL* **162** (Dec., 1970) L181.

- [36] A. K. Harding and R. Ramaty, *The Pulsar Contribution to Galactic Cosmic Ray Positrons*, in *International Cosmic Ray Conference*, vol. 2 of *International Cosmic Ray Conference*, p. 92, 1987.
- [37] J. Arons, *Pulsars as Gamma-Rays Sources: Nebular Shocks and Magnetospheric Gaps*, *SSRv* **75** (Jan., 1996) 235–255.
- [38] L. Zhang and K. S. Cheng, *Cosmic-ray positrons from mature gamma-ray pulsars*, *A&A* **368** (Mar., 2001) 1063–1070.
- [39] E. Amato, *The theory of pulsar wind nebulae*, [arXiv:1312.5945](https://arxiv.org/abs/1312.5945).
- [40] S. Della Torre, M. Gervasi, P. Rancoita, D. Rozza, and A. Treves, *Possible Contribution to Electron and Positron Fluxes from Pulsars and their Nebulae*, *ArXiv e-prints* (Dec., 2013) [[arXiv:1312.3483](https://arxiv.org/abs/1312.3483)].
- [41] M. Ruderman and P. Sutherland, *Theory of pulsars: Polar caps, sparks, and coherent microwave radiation*, *AJ* **196** (1975) 51.
- [42] A. Cheng, M. Ruderman, and P. Sutherland, *Current flow in pulsar magnetospheres*, *ApJ* **203** (Jan., 1976) 209–212.
- [43] K. Cheng, C. Ho, and M. A. Ruderman, *Energetic Radiation from Rapidly Spinning Pulsars. 1. Outer Magnetosphere Gaps. 2. Vela and Crab*, *AJ* **300** (1986) 500–539.
- [44] J. H. Taylor, R. N. Manchester, and A. G. Lyne, *Catalog of 558 pulsars*, *ApJS* **88** (Oct., 1993) 529–568.
- [45] M. Cirelli, G. Corcella, A. Hektor, G. Hutsi, M. Kadastik, et al., *PPPC 4 DM ID: A Poor Particle Physicist Cookbook for Dark Matter Indirect Detection*, *JCAP* **1103** (2011) 051, [[arXiv:1012.4515](https://arxiv.org/abs/1012.4515)].
- [46] P. Ciafaloni, D. Comelli, A. Riotto, F. Sala, A. Strumia, et al., *Weak Corrections are Relevant for Dark Matter Indirect Detection*, *JCAP* **1103** (2011) 019, [[arXiv:1009.0224](https://arxiv.org/abs/1009.0224)].
- [47] X. H. Sun, W. Reich, A. Waelkens, and T. Enslin, *Radio observational constraints on Galactic 3D-emission models*, *Astron. Astrophys.* **477** (2008) 573, [[arXiv:0711.1572](https://arxiv.org/abs/0711.1572)].
- [48] T. Delahaye, J. Laval, R. Lineros, F. Donato, and N. Fornengo, *Galactic electrons and positrons at the Earth: new estimate of the primary and secondary fluxes*, *A&A* **524** (Dec., 2010) A51, [[arXiv:1002.1910](https://arxiv.org/abs/1002.1910)].
- [49] D. Maurin, F. Donato, R. Taillet, and P. Salati, *Cosmic Rays below Z=30 in a Diffusion Model: New Constraints on Propagation Parameters*, *ApJ* **555** (July, 2001) 585–596, [[astro-ph/0101231](https://arxiv.org/abs/astro-ph/0101231)].
- [50] F. Donato, N. Fornengo, D. Maurin, P. Salati, and R. Taillet, *Antiprotons in cosmic rays from neutralino annihilation*, *Phy.Rev.D* **69** (Mar., 2004) 063501, [[astro-ph/0306207](https://arxiv.org/abs/astro-ph/0306207)].
- [51] L. A. Fisk, *Solar modulation of galactic cosmic rays, 2*, *JGR* **76** (1971) 221.
- [52] J. S. Perko, *Solar modulation of galactic antiprotons*, *A&A* **184** (Oct., 1987) 119–121.
- [53] M. Aguilar, D. Aisa, A. Alvino, G. Ambrosi, K. Andeen, L. Arruda, N. Attig, P. Azzarello, A. Bachlechner, F. Barao, and et al., *Electron and Positron Fluxes in Primary Cosmic Rays Measured with the Alpha Magnetic Spectrometer on the International Space Station*, *Physical Review Letters* **113** (Sept., 2014) 121102.
- [54] M. Aguilar, D. Aisa, B. Alpat, A. Alvino, G. Ambrosi, K. Andeen, L. Arruda, N. Attig, P. Azzarello, A. Bachlechner, and et al., *Precision Measurement of the $(e^+ + e^-)$ Flux in Primary Cosmic Rays from 0.5 GeV to 1 TeV with the Alpha Magnetic Spectrometer on the International Space Station*, *Physical Review Letters* **113** (Nov., 2014) 221102.
- [55] L. Accardo, M. Aguilar, D. Aisa, A. Alvino, G. Ambrosi, K. Andeen, L. Arruda, N. Attig, P. Azzarello, A. Bachlechner, and et al., *High Statistics Measurement of the Positron Fraction*

in Primary Cosmic Rays of 0.5-500 GeV with the Alpha Magnetic Spectrometer on the International Space Station, *Physical Review Letters* **113** (Sept., 2014) 121101.

- [56] A. Lewis and S. Bridle, *Cosmological parameters from CMB and other data: a Monte- Carlo approach*, *Phys. Rev.* **D66** (2002) 103511, [[astro-ph/0205436](#)].
- [57] M. Aguilar and et al., *Precision Measurement of the Proton Flux in Primary Cosmic Rays from Rigidity 1 GV to 1.8 TV with the Alpha Magnetic Spectrometer on the International Space Station*, *PRL* **114** (May, 2015) 171103.
- [58] M. Ackermann et al., *Measurement of Separate Cosmic-Ray Electron and Positron Spectra with the Fermi Large Area Telescope*, *PRL* **108** (Jan., 2012) 011103.
- [59] M. Ackermann, M. Ajello, W. B. Atwood, L. Baldini, et al., *Fermi LAT observations of cosmic-ray electrons from 7 GeV to 1 TeV*, *Phy.Rev.D* **82** (Nov., 2010) 092004, [[arXiv:1008.3999](#)].
- [60] O. Adriani, G. C. Barbarino, G. A. Bazilevskaya, et al., *An anomalous positron abundance in cosmic rays with energies 1.5-100GeV*, *Nature* **458** (Apr., 2009) 607–609, [[arXiv:0810.4995](#)].
- [61] O. Adriani, G. C. Barbarino, G. A. Bazilevskaya, et al., *Cosmic-Ray Electron Flux Measured by the PAMELA Experiment between 1 and 625 GeV*, *Phys.Rev.Lett.* **106** (May, 2011) 201101, [[arXiv:1103.2880](#)].
- [62] PAMELA Collaboration, *The cosmic-ray positron energy spectrum measured by PAMELA*, *ArXiv e-prints* (Aug., 2013) [[arXiv:1308.0133](#)].
- [63] F. Aharonian, A. G. Akhperjanian, et al., *Probing the ATIC peak in the cosmic-ray electron spectrum with H.E.S.S.*, *A&A* **508** (Dec., 2009) 561–564, [[arXiv:0905.0105](#)].
- [64] D. R. Lorimer, *The Galactic Population and Birth Rate of Radio Pulsars*, in *Young Neutron Stars and Their Environments* (F. Camilo and B. M. Gaensler, eds.), vol. 218 of *IAU Symposium*, p. 105, 2004. [[astro-ph/0308501](#)].
- [65] T. Delahaye, R. Lineros, F. Donato, N. Fornengo, and P. Salati, *Positrons from dark matter annihilation in the galactic halo: Theoretical uncertainties*, *Phys.Rev.* **D77** (2008) 063527, [[arXiv:0712.2312](#)].
- [66] T. Bringmann, F. Calore, M. Di Mauro, and F. Donato, *Constraining dark matter annihilation with the isotropic gamma-ray background: updated limits and future potential*, *Phys.Rev.* **D89** (2014), no. 2 023012.
- [67] M. Di Mauro and F. Donato, *Composition of the Fermi-LAT isotropic gamma-ray background intensity: Emission from extragalactic point sources and dark matter annihilations*, *Phys.Rev.* **D91** (2015) 123001, [[arXiv:1501.0531](#)].
- [68] T. R. Slatyer, *Indirect Dark Matter Signatures in the Cosmic Dark Ages I. Generalizing the Bound on s-wave Dark Matter Annihilation from Planck*, [[arXiv:1506.0381](#)].
- [69] S. Galli, F. Iocco, G. Bertone, and A. Melchiorri, *Updated CMB constraints on Dark Matter annihilation cross-sections*, *Phys. Rev.* **D84** (2011) 027302, [[arXiv:1106.1528](#)].